Classical Spin Liquid or Extended Critical Range in h-$YMnO_3$?

Sofie Janas,[1,2] Jakob Lass,[1,3] Ana-Elena Ţuţueanu,[1,4] Morten L. Haubro,[1] Christof Niedermayer,[3] Uwe Stuhr,[3] Guangyong Xu,[5] Dharmalingam Prabhakaran,[6] Pascale P. Deen,[7,1] Sonja Holm-Dahlin,[1,8] and Kim Lefmann[1,*]

[1]*Nanoscience Center, Niels Bohr Institute, University of Copenhagen, 2100 Copenhagen Ø, Denmark*
[2]*Institute of Physics, École Polytechnique Fédérale de Lausanne, CH-1015 Lausanne, Switzerland*
[3]*Laboratory for Neutron Scattering, Paul Scherrer Institute (PSI), 5232 Villigen, Switzerland*
[4]*Institut Laue-Langevin (ILL), Grenoble Cedex 9 38042, France*
[5]*NIST Center for Neutron Research, National Institute of Standards and Technology, Gaithersburg, Maryland 20899, USA*
[6]*Clarendon Laboratory, Department of Physics, University of Oxford, Oxford OX1 3PU, United Kingdom*
[7]*European Spallation Source ESS ERIC, Box 176, SE-221 00 Lund, Sweden*
[8]*ISIS Facility Rutherford Appleton Laboratory Chilton, Didcot, OX 11 OQX, United Kingdom*

(Received 8 June 2020; accepted 13 January 2021; published 11 March 2021)

Neutron spectroscopy on the classical triangular-lattice frustrated antiferromagnet h-$YMnO_3$ reveals diffuse, gapless magnetic excitations present both far below and above the ordering temperature. The correlation length of the excitations increases as the temperature approaches zero, bearing a strong resemblance to critical scattering. We model the dynamics in the ordered and correlated disordered phase as critical spin correlations in a two-dimensional magnetic state. We propose that our findings may provide a general framework to understand features often attributed to classical spin liquids.

DOI: 10.1103/PhysRevLett.126.107203

Frustrated magnetism, in which competing exchange interactions suppress magnetic order, is ubiquitous within condensed matter physics. One of the most heavily discussed topics is quantum spin liquids (QSLs), which are defined as fluidlike states, where the spins are highly correlated and continue to fluctuate down to temperatures of absolute zero [1–4], although experimental verification is still contentious. Many frustrated compounds show features reminiscent of QSLs but order magnetically at finite temperatures, which excludes them as QSL candidates. Above this ordering these compounds are referred to as classical spin liquids [4,5], as cooperative paramagnets [2], or merely as having spin-liquid-like phases [6], although no clear definition of these terms is readily available.

The classical triangular-lattice Heisenberg antiferromagnet with nearest-neighbor exchange interactions (TLHA) is one of the simplest geometrical motifs to exhibit frustration, although the TLHA has been shown to have an ordered ground state at $T = 0$ in both the quantum and classical spin case [7,8]. In this Letter, we study the hexagonal rare-earth manganite $YMnO_3$, which has stacked triangular-lattice planes and is a close approximation to a TLHA with classical spins. h-$YMnO_3$ is also widely studied due to its type-I multiferroic nature. In h-$YMnO_3$, the localized $S = 2$ spin on the Mn^{3+} ions form a two-dimensional triangular lattice [see Fig. 1(a)], separated by interlayer Y and O ions. h-$YMnO_3$ has a Curie-Weiss temperature of $\theta_{CW} = -545$ K [6] and a magnetic phase transition to a three-dimensionally ordered antiferromagnetic state at $T_N = 71$ K [9,10]. Its magnetic interactions are dominantly an antiferromagnetic Heisenberg nearest-neighbor exchange, $J = 2.4$ meV, with a weaker easy-plane anisotropy within the hexagonal plane with $D/J \approx 0.13$ and even weaker interlayer interactions, $J_z/J \approx 0.06$ [11], thus making h-$YMnO_3$ highly two-dimensional and TLHA-like. The magnetic ordering below T_N within the triangular planes is the 120° spin structure shown in Fig. 1(a).

Diffuse scattering in h-$YMnO_3$ above T_N observed via neutron spectroscopy was previously reported by some groups on both powders and single crystals [9,13–17] and was ascribed to a spin-liquid state. However, no systematic studies such as temperature and energy dependencies of the signal were performed, and a coherent understanding and modeling of these features is still absent. Here, we show that the spin-liquid-like features in the TLHA of hexagonal $YMnO_3$ can be modeled as arising from critical scattering in a vastly extended temperature regime due to its geometrical frustration. This may provide a general framework for the understanding of frustration in TLHA and similar systems.

Neutron spectroscopy directly probes the magnetic dynamic structure factor $S(\mathbf{Q}, \omega)$ as a function of scattering wave vector $\mathbf{Q}$ and energy transfer $\hbar\omega$ [18]. Our experiments were performed on a 3.4 g single crystal of h-$YMnO_3$ aligned in the $(hk0)$ plane. To obtain an overview of the excitations, we used the cold-neutron spectrometer CAMEA (PSI) [19–21] that utilizes multiplexing analyzers and a large detector array to obtain quasicontinuous coverage in three-dimensional $(h, k, \hbar\omega)$ space. The data [Figs. 1(c)–1(f)] are taken at $T = 60$ K ($< T_N$) and at

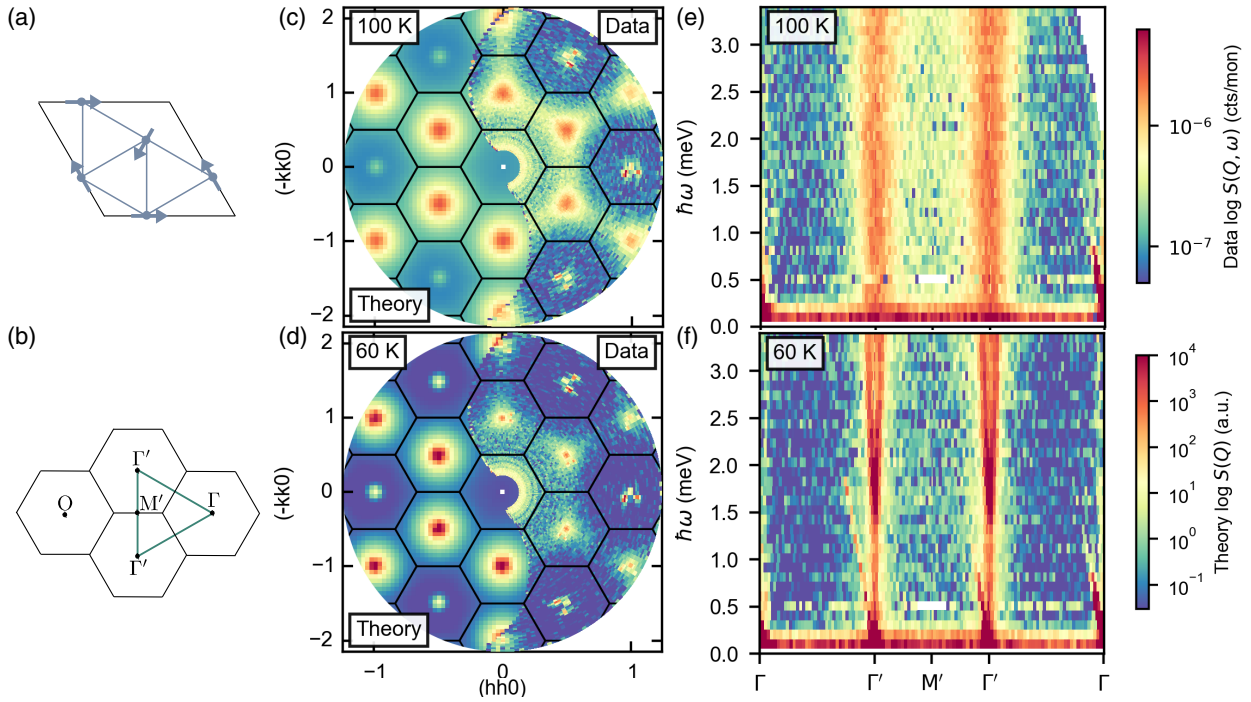

FIG. 1. (a) The spin structure of h-$YMnO_3$ in the two-dimensional triangular lattice with Mn spins in the 120° structure. (b) Sketch of the reciprocal lattice. Γ' is a magnetic Bragg peak, Γ is a structural Bragg peak, and M' is the center of the Brillouin edge between neighboring magnetic Bragg reflections. Green lines indicate the direction of the $\mathbf{Q}$ cut used in (e) and (f). (c)–(f) Color maps of inelastic neutron data on h-$YMnO_3$ measured above and below T_N on a common, logarithmic intensity scale, created with the software MJOLNIR [12]. (c) and (d) show constant-energy cuts at $\hbar\omega = 1 \pm 0.2$ meV for $T = 100$ K and $T = 60$ K, respectively, compared with numerical simulations of the scattering as critical fluctuations. The model is described in the text and plotted on its own logarithmic intensity scale. (e),(f) $(\mathbf{Q}, \hbar\omega)$ cuts of the same experimental data along the green line in (b) with binning 0.1 meV and 0.05 Å.

$T = 100$ K ($> T_N$). Constant-energy maps with $\hbar\omega = 1.0 \pm 0.2$ meV are shown in Figs. 1(c) and 1(d), superimposed on a theoretical simulation described later. Figures 1(e) and 1(f) show $(\mathbf{Q}, \hbar\omega)$ cuts of the same data across two magnetic Bragg reflections. The cut direction is sketched in Fig. 1(b). In the constant-energy map for 100 K in Fig. 1(c), we observe a diffuse signal. Broad peaks of higher intensity reside at Γ', consistent with the location of magnetic Bragg peaks below T_N. These peaks are connected with sheets of diffuse scattering crossing the M' points to form a hexagonal pattern. The signal is strongest for small Q, as expected due to the magnetic form factor [18]. Figure 1(d) shows that the scattering for $T = 60$ K ($< T_N$) is very similar to that at 100 K, although less intense, and the peaks are narrower, indicating longer-ranged correlations. In the data, Currat-Axe spurions [18,22] can be seen as two narrow, bright peaks, close to the Bragg peaks in Figs. 1(c) and 1(d), and as sharp, linearly dispersing streaks in Figs. 1(e) and 1(f).

In the $(\mathbf{Q}, \hbar\omega)$ cut at 100 K [Fig. 1(e)], the Γ' excitation is seen as broad rods with approximately constant intensity and width for increasing energy. The rods are gapless within energy resolution, $\Delta E \sim 0.2$ meV. The M' excitation is seen as increased intensity between the two Γ' points and also appears featureless with energy-independent intensity. Below T_N [Fig. 1(f)], a spin wave is seen as a steep parabolic shape that has its bottom at the Γ' point, at $\hbar\omega \approx 1.7$ meV $= \Delta$. The spin-wave gap Δ is due to the single-ion anisotropy of h-$YMnO_3$ [10,27,28]. However, the intensity below Δ is not associated with any spin wave, and we recognize this important feature as the same diffuse signal as above T_N, although it is narrowed below T_N.

Based on this, we carried out detailed studies of the temperature and energy dependencies of the excitations using combined data from triple-axis spectrometers (TAS). We utilized the thermal TAS Eiger (PSI) [29] and IN3 (ILL) with $\Delta E \sim 1$ meV. The cold TAS SPINS (NIST) with better resolution, $\Delta E \sim 0.2$ meV, was used to access the excitation below the spin-wave gap in the ordered phase. The intensities have been cross-normalized between instruments; see [22].

We investigated the temperature dependence of the peak intensities and widths by constant-energy scans through Γ' with $\hbar\omega = 1$ meV at SPINS and through M' with $\hbar\omega = 5$ meV at Eiger and IN3. The scan directions are shown in the inset in Fig. 2(b). Each dataset is fitted with a Lorentzian, and the integrated intensity and real-space correlation lengths ξ are shown in Figs. 2(a) and 3(b) for both Γ' and M'.

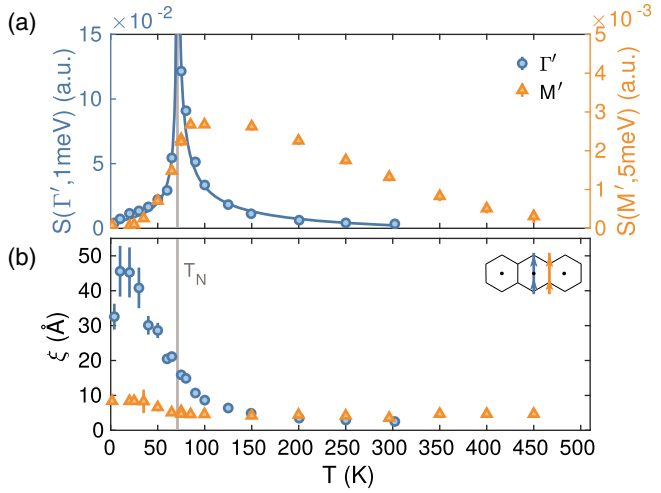

FIG. 2. Temperature dependence of (a) the integrated intensity and (b) the correlation length for Γ' and M' from neutron spectroscopy. Scan directions are shown schematically in (b). Full blue lines are power-law fits to Γ' data.

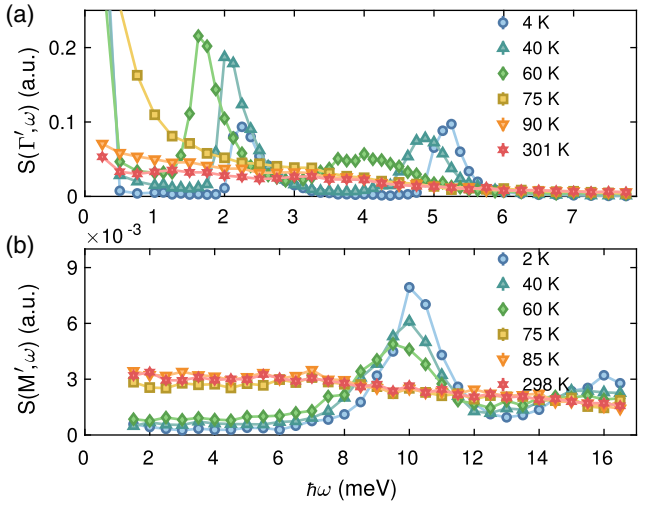

FIG. 3. Energy dependence of diffuse excitations at Γ' (a) and at M' (b) from neutron spectroscopy.

The integrated intensity at Γ' [Fig. 2(a)] increases quickly when approaching T_N. The resemblance to a divergence at T_N is illustrated by a power law fitted to the Γ' data. The Γ' excitation is well defined at both the highest (301 K $\approx 4.2T_N$) and lowest (4 K $\approx 0.06T_N$) temperatures accessed and is more intense than the M' excitation. The integrated intensity at M' is at background level below 25 K and quickly increases in intensity upon heating through T_N. Above T_N, the intensity decreases very slowly, reaching background level at 450 K, close to $|\theta_{\mathrm{CW}}| = 545$ K. The correlation length for the Γ' excitation above T_N is $\xi \approx 4$ Å [see Fig. 2(b)], similar to the interatomic distance between neighboring Mn atoms, 3.53 Å. When cooling below T_N, the correlation length increases smoothly to 45 Å, which is approximately the resolution limit. Curiously, no divergence in ξ is found at T_N, and instead ξ increases with decreasing temperature. The correlation length of the M' excitations [Fig. 2(b)] is approximately constant at 4 Å for the entire temperature range, matching the high-temperature correlation length of Γ'.

The energy dependence of the diffuse excitations was investigated at different temperatures by constant-Q scans at Γ' and M'; see Fig. 3. The Γ' intensity at 4 K [Fig. 3(a)] shows two magnon modes at 2.2 meV and at 5.2 meV [11,30]. With increasing temperatures, the magnons soften [10], but, in addition, diffuse intensity appears. At 75 K, just above T_N, quasielastic, critical fluctuations are seen close to the three-dimensional phase transition. This behavior subsides already for 90 K, above which the diffuse excitation has roughly constant intensity up to 4 meV, where it eventually vanishes at 6 meV. For M' at 2 K [see Fig. 3(b)], magnons are seen at 10 and 16 meV [11,30]. Increasing the temperature broadens and weakens the magnons and increases the diffuse signal. Upon crossing T_N, a sudden jump is observed in the intensity, which becomes almost energy independent. This behavior is unchanged up to 300 K.

The inelastic signal at Γ' exhibits a divergence in intensity at T_N and a spike in correlation length at low temperatures with similarities to a divergence at $T = 0$. The smooth energy dependence of the fluctuations above T_N corresponds to fluctuations on all timescales below the characteristic energy scale zJS, where $z = 6$ is the number of nearest neighbors. These features are spin-liquid-like due to the resemblance to the diffuse fractionalization which is an experimental fingerprint of quantum spin liquids [1,2]. However, the diverging intensities and correlation lengths also resemble features of critical scattering: Around a phase transition, there will be diffuse, quasielastic scattering whose intensity and correlation length diverge at the transition temperature [18,31]. For unfrustrated magnets, this typically happens in a temperature range of ~5%–10% of T_N, where diffuse scattering sharpens to form Bragg reflections. If the measured excitations followed this trend, they should have a pronounced intensity variation along the l direction.

To investigate this dimensionality of the diffuse excitations, we investigated the M' excitation for different l values on a smaller sample aligned in the (hhl) scattering plane on IN3; see [22]. Both integrated intensity and width appear independent of l at temperatures 70 and 100 K; see Fig. 4. This indicates that the diffuse scattering is a two-dimensional phenomenon within the triangular-lattice plane and does not contribute to the formation of Bragg reflections from three-dimensional order. Thus, the excitations arise from in-plane correlations without contribution from interlayer correlations, proving that the M' signals do not arise from simple critical scattering. However, they could be caused by critical scattering from the suppressed

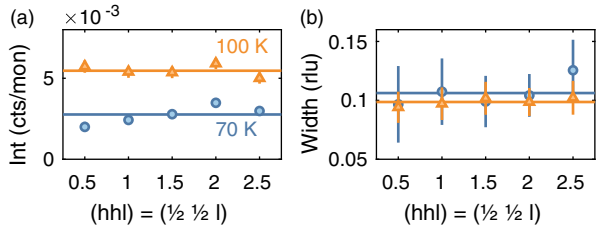

FIG. 4. Integrated intensity (a) and width (b) of the M' excitation measured for different l values. Scans across the excitation at 70 and 100 K were fitted with a Lorentzian. Full lines indicate the mean value of parameters.

two-dimensional order, which would appear at $T = 0$ in an idealized TLHA system. In this scenario, the critical range is vastly extended compared to the critical range around T_N due to the strength of the interactions, while the order is suppressed by geometric frustration.

Investigating this similarity, we model our data as critical scattering from correlated clusters populated with spins in the two-dimensional 120° ground state that fluctuate coherently. In this simple model, the Q dependence of the dynamical structure factor equals that of the static structure factor:

$$S(\mathbf{Q}) = f(Q)^2 \sum_{l=0}^{N} \sum_{\alpha,\beta} e^{i\mathbf{Q}\cdot\mathbf{r}_l} (\delta_{\alpha,\beta} - \hat{Q}_\alpha \hat{Q}_\beta) \langle S_0^\alpha S_l^\beta \rangle, \quad (1)$$

where N is the number of spins, α and β are the x, y, z vector components, $f(Q)$ is the magnetic form factor for Mn^{3+}, $\mathbf{r}_l$ is their position in the lattice, S_l^α refers to their spin component, and the brackets $\langle \cdots \rangle$ refers to a 4π rotational average.

The cluster structure is typically taken as the minimal geometrical motif in the lattice [32], which here is the spin trimer. However, since our correlation lengths extend beyond the nearest neighbor, we instead simulate a larger supercell. Under the assumption of critical scattering in the two-dimensional planes, we incorporate the spin-spin correlation by the critical form $\langle S_0 S_l \rangle \propto \exp(-|\mathbf{r}_{0l}|/\xi)$ [31]. Using the temperature-dependent correlation lengths determined for Γ', $\xi(100\ \mathrm{K}) = 8.6$ Å and $\xi(60\ \mathrm{K}) = 20.5$ Å, we set up a supercell of 60×60 unit cells consisting of 10 800 spins to achieve the $S(\mathbf{Q})$ spectra shown alongside the data in Figs. 1(c) and 1(d). The simulations qualitatively reproduce the experimental data. In Fig. 1, both measured and simulated $S(\mathbf{Q})$ are plotted on a logarithmic color scale. However, the simulated scale spans more decades than the experimental data, and the peaks have a circularly symmetric shape rather than the slightly triangular seen in the data. We attribute this to the simplicity of our model, which is energy integrated and does not take the Hamiltonian into account. Calculations based on the microscopic Hamiltonian will reproduce the triangular nature of the data, e.g., spin-wave theory [33] and the calculations in Refs. [34,35]. Nevertheless, the simulation matches the data well, with strong peaks at Γ', which are connected by weaker sheets of intensity across M'. A scan perpendicular to the sheets shows a peaked profile; see [22]. This allows us to conclude that the Γ' and M' excitations arise from the same origin despite the different temperature and energy dependencies. Additionally, the large cluster with exponentially decaying spin-spin correlations much better captures the experimental features than the simple trimer model [22].

We envision the following physical picture for the short-range dynamics in TLHAs: Spins on the lattice develop local 120° in-plane correlations below θ_{CW}, giving rise to diffuse scattering from the dynamic correlated disorder. These magnetic clusters are subject to thermal noise and fluctuate on all relevant timescales. With decreasing temperature, the typical size of the spin clusters, ξ, increases, resulting in increased scattering intensity. At T_N, the coupling between the layers causes a three-dimensional magnetic ordering, from which collective spin waves emerge that coexist with the spin cluster excitations. Thus, order coexists with correlated disorder below T_N. Indeed, in the limit $T \to 0$, the size of the clusters increases. Meanwhile, the intensity of the fluctuations diminishes, because the static magnetic ordering becomes more pronounced, leaving less spectral weight for the diffuse excitations. Since the fluctuations of the clusters happen at all timescales, in contrast to the well-defined frequencies of spin waves, we believe that these two dynamic phenomena are decoupled and at most weakly interacting.

For h-$YMnO_3$, the vastly extended critical range has profound consequences on the physical properties, as evidenced by the anomalous thermal conductivity κ in the temperature range between 20 and 300 K [36]. This could not explained by the usual phononic terms, whence the anomalies are proposed to be caused by short-ranged magnetic excitations coupled to the heat-carrying phonons via exchange striction [36]. The anomalous temperature range corresponds well to the temperature range where we observe strong critical fluctuations. For this reason, we speculate that it is indeed these short-ranged critical fluctuations that dynamically couple to the phonons and cause the thermal conductivity anomalies.

Anomalous values have also been reported for the critical exponent β in h-$YMnO_3$ [9,10] and other TLHA materials, such as VCl_2 [37,38], that do not correspond to any of the well-known universality classes. We speculate that this is caused by the presence of the two-dimensional, dynamic correlated disorder which moves the phase transition beyond the simple Landau regime.

Scattering patterns reminiscent of our experimental data have been reported in theoretical studies of the purely two-dimensional TLHA, which were based on exponential tensor renormalization group theory for quantum spins [34] and Monte Carlo simulations on classical spins [35].

Both studies obtain diffuse scattering maps consistent with ours. Notably, Chen *et al.* [34] observe a temperature dependence of the scattering intensities analogous to our experimental data, when ignoring the presence of a finite-temperature magnetic phase transition. We take these theoretical results as further evidence that the diffuse scattering stems purely from the two-dimensional 120° order. Some groups have put forth more exotic explanations for the cause of the diffuse scattering, such as Z_2 spin vortices [35,39] and chiral rotonlike excitations [34]. Chiral rotons should be gapped [34] and should have clear dispersions with rotons as local minima [40]. Our data put an upper bound of 0.2 meV on any gap in the non-spin-wave excitations and show the excitations to have a vertical dispersion with no dips. Furthermore, a Z_2 spin vortex cannot be accommodated with our observed short correlation lengths. Based on this, we do not find any evidence for these two origins in our data.

Our experiments on h-$YMnO_3$ provide evidence for two-dimensional critical scattering as the origin of low-lying, diffuse scattering observed in triangular-lattice antiferromagnets. The diffuse scattering comes from dynamic correlated disorder of spins, coexisting with the ordered state below T_N. Diffuse excitations similar to ours have been observed in other geometrically frustrated magnets, such as the classical spin systems $CuCrO_2$ [41] and $MgCr_2O_4$ [5], as well as in quantum spin systems herbertsmithite [42] and $YbMgGaO_4$ [43,44]. These spectra also show diffuse, gapless excitations without any sharp features [1] and have been referred to as (classical and quantum) spin liquids. However, we show that in the classical h-$YMnO_3$ the excitations can be satisfactorily modeled by critical spin fluctuations existing in a vastly extended critical region due to the frustration. Thus, it seems worth contemplating whether such features in other compounds can also be modeled by critical fluctuations, which may, in general, enable a more precise definition of the term "classical spin liquid".

This work was supported by the Danish Agency for Research and Innovation through the DANSCATT Grant No. 7055-00010B and the United Kingdom Engineering and Physical Sciences Research Council Grant No. EP/M020517/1. The neutron experiments were performed at the Paul Scherrer Institute (Switzerland), at the Institute Laue Langevin (France), and at the National Institute of Standards and Technology (NIST) Center for Neutron Research (United States). We thank Nicola Spaldin and Bruce Gaulin for helpful discussions.

*Corresponding author.
lefmann@nbi.ku.dk

[1] L. Savary and L. Balents, Quantum spin liquids: a review, Rep. Prog. Phys. **80**, 016502 (2017).
[2] J. Knolle and R. Moessner, A field guide to spin liquids, Annu. Rev. Condens. Matter Phys. **10**, 451 (2019).
[3] X. G. Wen, Quantum orders and symmetric spin liquids, Phys. Rev. B **65**, 165113 (2002).
[4] L. Balents, Spin liquids in frustrated magnets, Nature (London) **464**, 199 (2010).
[5] X. Bai, J. A. M. Paddison, E. Kapit, S. M. Koohpayeh, J. J. Wen, S. E. Dutton, A. T. Savici, A. I. Kolesnikov, G. E. Granroth, C. L. Broholm, J. T. Chalker, and M. Mourigal, Magnetic Excitations of the Classical Spin Liquid $MgCr_2O_4$, Phys. Rev. Lett. **122**, 097201 (2019).
[6] J. Park, J.-G. Park, G. S. Jeon, H.-Y. Choi, C. Lee, W. Jo, R. Bewley, K. A. McEwen, and T. G. Perring, Magnetic ordering and spin-liquid state of $YMnO_3$, Phys. Rev. B **68**, 104426 (2003).
[7] B. Bernu, C. Lhuillier, and L. Pierre, Signature of Néel Order in Exact Spectra of Quantum Antiferromagnets on Finite Lattices, Phys. Rev. Lett. **69**, 2590 (1992).
[8] L. Capriotti, A. E. Trumper, and S. Sorella, Long-Range Néel Order in the Triangular Heisenberg Model, Phys. Rev. Lett. **82**, 3899 (1999).
[9] B. Roessli, S. N. Gvasaliya, E. Pomjakushina, and K. Conder, Spin fluctuations in the stacked-triangular antiferromagnet $YMnO_3$, JETP Lett. **81**, 287 (2005).
[10] S. Holm-Dahlin, S. Janas, A. Kreisel, E. Pomjakushina, J. White, A. Fennell, and K. Lefmann, The magnetic phase transition and universality class of h-$YMnO_3$ and h-$(Y_{0.98}Eu_{0.02})MnO_3$ under zero and applied pressure, Quantum Beam Sci. **2**, 16 (2018).
[11] S. L. Holm, A. Kreisel, T. K. Schäffer, A. Bakke, M. Bertelsen, U. B. Hansen, M. Retuerto, J. Larsen, D. Prabhakaran, P. P. Deen, Z. Yamani, J. O. Birk, U. Stuhr, C. Niedermayer, A. L. Fennell, B. M. Andersen, and K. Lefmann, Magnetic ground state and magnon-phonon interaction in multiferroic h-$YMnO_3$, Phys. Rev. B **97**, 134304 (2018).
[12] J. Lass, H. Jacobsen, D. G. Mazzone, and K. Lefmann, MJOLNIR: A software package for multiplexing neutron spectrometers, arXiv:2007.14816.
[13] T. J. Sato, S.-H. Lee, T. Katsufuji, M. Masaki, S. Park, J. R. D. Copley, and H. Takagi, Unconventional spin fluctuations in the hexagonal antiferromagnet $YMnO_3$, Phys. Rev. B **68**, 014432 (2003).
[14] T. Chatterji, S. Ghosh, A. Singh, L. P. Regnault, and M. Rheinstädter, Spin dynamics of $YMnO_3$ studied via inelastic neutron scattering and the anisotropic Hubbard model, Phys. Rev. B **76**, 144406 (2007).
[15] D. P. Kozlenko, I. Mirebaeu, J.-G. Park, I. N. Goncharenko, S. Lee, J. Park, and B. N. Savenko, High-pressure-induced spin-liquid phase of multiferroic $YMnO_3$, Phys. Rev. B **78**, 054401 (2008).
[16] F. Demmel and T. Chatterji, Persistent spin waves above the Néel temperature in $YMnO_3$, Phys. Rev. B **76**, 212402 (2007).
[17] T. Lonkai, D. G. Tomuta, J.-U. Hoffmann, R. Schneider, D. Hohlwein, and J. Ihringer, Magnetic two-dimensional short-range order in hexagonal manganites, J. Appl. Phys. **93**, 8191 (2003).
[18] G. Shirane, S. M. Shapiro, and J. M. Tranquada, *Neutron Scattering with a Triple-Axis Spectrometer* (Cambridge University Press, Cambridge, England, 2013).

[19] F. Groitl, D. Graf, J. O. Birk, M. Markó, M. Bartkowiak, U. Filges, C. Niedermayer, C. Rüegg, and H. M. Rønnow, CAMEA—A novel multiplexing analyzer for neutron spectroscopy, Rev. Sci. Instrum. **87**, 035109 (2016).

[20] J. Lass, D. Graf, F. Groitl, K. Christian, R. Bürge, R. Müller, P. Keller, F. Herzog, U. Greuter, G. Theidel, L. Testa, V. Favre, H. M. Rønnow, and C. Niedermayer, Design and performance of the multiplexing spectrometer CAMEA, arXiv:2007.14796.

[21] J. O. Birk, M. Markó, P. G. Freeman, J. Jacobsen, R. L. Hansen, N. B. Christensen, C. Niedermayer, M. Månsson, H. M. Rønnow, and K. Lefmann, Prismatic analyser concept for neutron spectrometers, Rev. Sci. Instrum. **85**, 113908 (2014).

[22] See Supplemental Material at http://link.aps.org/supplemental/10.1103/PhysRevLett.126.107203 for further experimental and simulation details, which includes Refs. [23–26].

[23] B. Lorenz, Hexagonal manganites: Strong coupling of ferroelectricity and magnetic orders, Phys. Sci. Rev. **4**, 20190014 (2019).

[24] M. Fiebig, D. Fröhlich, K. Kohn, St. Leute, Th. Lottermoser, V. V. Pavlov, and R. V. Pisarev, Determination of the Magnetic Symmetry of Hexagonal Manganites by Second Harmonic Generation, Phys. Rev. Lett. **84**, 5620 (2000).

[25] C. J. Howard, B. J. Campbell, H. T. Stokes, M. A. Carpenter, and R. I. Thomson, Crystal and magnetic structures of hexagonal $YMnO_3$, Acta Crystallogr. Sect. B **69**, 534 (2013).

[26] T. Lancaster, S. J. Blundell, D. Andreica, M. Janoschek, B. Roessli, S. N. Gvasaliya, K. Conder, E. Pomjakushina, M. L. Brooks, P. J. Baker, D. Prabhakaran, W. Hayes, and F. L. Pratt, Magnetism in Geometrically Frustrated $YMnO_3$ under Hydrostatic Pressure Studied with Muon Spin Relaxation, Phys. Rev. Lett. **98**, 197203 (2007).

[27] S. Petit, F. Moussa, M. Hennion, S. Pailhès, L. Pinsard-Gaudart, and A. Ivanov, Spin Phonon Coupling in Hexagonal Multiferroic $YMnO_3$, Phys. Rev. Lett. **99**, 266604 (2007).

[28] H. Sim, J. Oh, J. Jeong, M. D. Le, and J. G. Park, Hexagonal $R$$MnO_3$: a model system for two-dimensional triangular lattice antiferromagnets, Acta Crystallogr. Sect. B **72**, 3 (2016).

[29] U. Stuhr, B. Roessli, S. Gvasaliya, H. Rønnow, U. Filges, D. Graf, A. Bollhalder, D. Hohl, R. Bürge, M. Schild, L. Holitzner, K. C., P. Keller, and T. Mühlebach, The thermal triple-axis-spectrometer EIGER at the continuous spallation source SINQ, Nucl. Instrum. Methods Phys. Res., Sect. A **853**, 16 (2017).

[30] J. Oh, M. D. Le, H. H. Nahm, H. Sim, J. Jeong, T. G. Perring, H. Woo, K. Nakajima, S. Ohira-Kawamura, Z. Yamani, Y. Yoshida, H. Eisaki, S. W. Cheong, A. L. Chernyshev, and J. G. Park, Spontaneous decays of magneto-elastic excitations in non-collinear antiferromagnet $(Y, Lu)MnO_3$, Nat. Commun. **7**, 13146 (2016).

[31] M. F. Collins, *Magnetic Critical Scattering* (Oxford University Press, Oxford, 1989).

[32] S. H. Lee, C. Broholm, W. Ratcliff, G. Gasparovic, Q. Huang, T. H. Kim, and S. W. Cheong, Emergent excitations in a geometrically frustrated magnet, Nature (London) **418**, 856 (2002).

[33] M. Mourigal, W. T. Fuhrman, A. L. Chernyshev, and M. E. Zhitomirsky, Dynamical structure factor of the triangular-lattice antiferromagnet, Phys. Rev. B **88**, 094407 (2013).

[34] L. Chen, D. W. Qu, H. Li, B. B. Chen, S. S. Gong, J. von Delft, A. Weichselbaum, and W. Li, Two-temperature scales in the triangular-lattice Heisenberg antiferromagnet, Phys. Rev. B **99**, 140404(R) (2019).

[35] T. Okubo and H. Kawamura, Signature of a Z_2 vortex in the dynamical correlations of the triangular-lattice Heisenberg antiferromagnet, J. Phys. Soc. Jpn. **79**, 084706 (2010).

[36] P. A. Sharma, J. S. Ahn, N. Hur, S. Park, S. B. Kim, S. Lee, J.-G. Park, S. Guha, and S.-W. Cheong, Thermal Conductivity of Geometrically Frustrated, Ferroelectric $YMnO_3$: Extraordinary Spin-Phonon Interactions, Phys. Rev. Lett. **93**, 177202 (2004).

[37] M. F. Collins and O. A. Petrenko, Review/Synthse: Triangular antiferromagnets, Can. J. Phys. **75**, 605 (1997).

[38] H. Kawamura, Universality of phase transitions of frustrated antiferromagnets, J. Phys. Condens. Matter **10**, 4707 (1998).

[39] H. Kawamura and S. Miyashita, Phase transition of the two-dimensional Heisenberg antiferromagnet on the triangular lattice, J. Phys. Soc. Jpn. **53**, 4138 (1984).

[40] S. Ito, N. Kurita, H. Tanaka, S. Ohira-Kawamura, K. Nakajima, S. Itoh, K. Kuwahara, and K. Kakurai, Structure of the magnetic excitations in the spin-1/2 triangular-lattice Heisenberg antiferromagnet $Ba_3CoSb_2O_9$, Nat. Commun. **8**, 235 (2017).

[41] R. Kajimoto, K. Tomiyasu, K. Nakajima, S. Ohira-Kawamura, Y. Inamura, and T. Okuda, Development of spin correlations in the geometrically frustrated triangular-lattice Heisenberg antiferromagnet $CuCrO_2$, J. Phys. Soc. Jpn. **84**, 074708 (2015).

[42] T. H. Han, J. S. Helton, S. Chu, D. G. Nocera, J. A. Rodriguez-Rivera, C. Broholm, and Y. S. Lee, Fractionalized excitations in the spin-liquid state of a kagome-lattice antiferromagnet, Nature (London) **492**, 406 (2012).

[43] Y. Shen, Y. D. Li, H. Wo, Y. Li, S. Shen, B. Pan, Q. Wang, H. C. Walker, P. Steffens, M. Boehm, Y. Hao, D. L. Quintero-Castro, L. W. Harriger, M. D. Frontzek, L. Hao, S. Meng, Q. Zhang, G. Chen, and J. Zhao, Evidence for a spinon Fermi surface in a triangular-lattice quantum-spin-liquid candidate, Nature (London) **540**, 559 (2016).

[44] J. A. Paddison, M. Daum, Z. Dun, G. Ehlers, Y. Liu, M. B. Stone, H. Zhou, and M. Mourigal, Continuous excitations of the triangular-lattice quantum spin liquid $YbMgGaO_4$, Nat. Phys. **13**, 117 (2017).